Elsevier Editorial System(tm) for Marine Geology
Manuscript Draft

Manuscript Number:

Title: Shallow water methane-derived authigenic carbonate mounds at the Codling Fault Zone, western Irish Sea

Article Type: Research Paper

Keywords: Methane-derived authigenic carbonate, gas seepage, Codling Fault, Irish Sea

Corresponding Author: Dr. Brian Kelleher,

Corresponding Author's Institution: Dublin City University

First Author: Shane S O'Reilly, PhD

Order of Authors: Shane S O'Reilly, PhD; Kryysztof Hryniewicz, PhD; Crispin T Little, PhD; Xavier Monteys, BSc; Michal T Szpak, PhD; Christopher C Allen, PhD; Brian Kelleher

Suggested Reviewers: Joseph Kelley
University of Maine
jtkelley@maine.maine.edu
A marine geologist who has research interests in phenomena like gas-escape pockmarks and cold-water carbonates.

Oyvind Hammer
Natural History Museum, University of Oslo
ohammer@nhm.uio.no
Expert in marine geology and biogeochemical processes:
http://www.nhm.uio.no/english/about/organization/research-collections/people/ohammer/

Richard Pancost
School of Chemistry,, University of Bristol
r.d.pancost@bristol.ac.uk
Expert in molecular and isotopic proxies for biogeochemical processes in modern and ancient sediments

Alan Judd
School of the Environment, University of Sunderland
alan.judd@sunderland.ac.uk
One of the world's foremost authorities on seafloor pockmarks and co-author of:
Seabed Fluid Flow
The Impact on Geology, Biology and the Marine Environment.

07 November 2013

Corresponding author:
Dr Brian Kelleher
School of Chemical Sciences
Dublin City University
Dublin 9
Ireland
Tel +353 1 7005134
Fax +353 1 700 5503
E-mail: brian.kelleher@dcu.ie

Title: Shallow water methane-derived authigenic carbonate mounds at the Codling Fault Zone, western Irish Sea

Dear Editor,

We are delighted to submit our manuscript to *Marine Geology*. This paper presents novel research into methane-derived authigenic carbonate (MDAC) mounds in the Codling Fault Zone (CFZ) in the Irish Sea. Isotopically depleted carbonate, with aragonite as the major authigenic mineral phase, together with the co-precipitation of framboidal pyrite confirm that anaerobic oxidation of methane (AOM) is an important process at the CFZ seeps. The isotopic depletion suggests a biogenic source, but thermogenic gas cannot be fully ruled out. Active seepage from one of the mounds was recorded, and extensive patches of reduced sediment indicates that seepage is ongoing. There is also evidence of significant dilution of the AOM process by organic matter from photosynthesis.
Thank you for your consideration of our manuscript. We look forward to your response.

Sincerely,

Brian Kelleher

Highlights

- An MDAC mound at the Codling Fault Zone, in the western Irish Sea was investigated.
- Isotopically depleted carbonate, aragonite, and framboidal pyrite confirm AOM.
- Isotopic depletion suggests biogenic source, but thermogenic gas cannot be ruled out.
- Ongoing seepage and mounds composed of stacked MDAC pavements.
- Significant dilution of the AOM process by organic matter from photosynthesis.

Shallow water methane-derived authigenic carbonate mounds at the Codling Fault Zone, western Irish Sea

Shane S. O'Reilly[a], Krzysztof Hryniewicz[b], Crispin T.S. Little[c], Xavier Monteys[d], Michal T. Szpak[a], Christopher C.R. Allen[e], Brian P. Kelleher[a*].

[a] *School of Chemical Sciences, Dublin City University, Glasnevin, Dublin 9, Ireland.*

[b] *Natural History Museum, University of Oslo, 1172 Blindern, 0316 Oslo, Norway.*

[c] *School of Earth Sciences, University of Leeds, Leeds LS2 9JT, United Kingdom.*

[d] *Geological Survey of Ireland, Beggars Bush, Haddington Road, Dublin 4, Ireland.*

[e] *School of Biological Sciences, Queen's University Belfast, University Road, Belfast BT7 1NN, United Kingdom.*

[*] *Corresponding author – Brian P Kelleher*

School of Chemical Sciences, Dublin City University, Glasnevin, Dublin 9, Ireland.

brian.kelleher@dcu.ie

Tel: 00353 1 7005134

Abstract

The process of anaerobic oxidation of methane (AOM) to methane-derived authigenic carbonate (MDAC) plays an important role in mediating marine methane release to the water column and atmosphere, and can facilitate distinct and often unique microbial and macrofaunal diversity. To date extensive MDAC with obligate microbial and macrofaunal diversity have been primarily reported in deep sea settings where organic carbon input from photosynthesis is limited. In this study mound features at the Codling Fault Zone (CFZ), located within the photic zone (50 to 120 m) of the western Irish Sea were investigated. Isotopically depleted carbonate, with aragonite as the major authigenic mineral phase, together with the co-precipitation of framboidal pyrite confirm that AOM is an important process at the CFZ seeps. The isotopic depletion of bulk carbonate and sampled gas suggests a biogenic source, however significant mixing of thermogenic gas and depletion of the original isotope signature cannot be ruled out. Active seepage from one of the mounds was recorded, and together with extensive patches of reduced sediment indicating that seepage is ongoing. The mounds appear to be composed of stacked MDAC pavements that are largely covered by sand and extensively eroded. The CFZ carbonates are colonized by abundant *Sabellaria* polychaetes and possible *Nemertesia* hydroids, which benefit indirectly from available hard substrate; seep specialist fauna are lacking. In contrast to most deep sea cold seep MDAC, analysis shows that organic matter from benthic and water column plankton microalgae dominate. This suggests that there is significant dilution of the AOM process by organic matter from photosynthesis at these shallow depths.

Keywords: Methane-derived authigenic carbonate, gas seepage, Codling Fault, Irish Sea

Abbreviations: Anaerobic oxidation of methane (AOM), Codling Fault Zone (CFZ), Dimethyl disulfide (DMDS), Energy-dispersive spectroscopy (EDS), Fatty acid methyl ester (FAME), Methane-derived authigenic carbonate (MDAC), Mono-alkyl glycerol ethers (MAGE), X-Ray diffraction (XRD).

1. Introduction

Methane is an important trace gas in the atmosphere and a potent greenhouse gas (Svensen et al., 2004; Forster et al., 2007). Seepage of methane from the ocean's seafloor is of global occurrence, yet one that is poorly quantified and understood (Fleischer et al., 2001; Knittel and Boetius, 2009). One result of seabed seepage is the formation of distinctive seafloor structures, such as pockmarks, mud diapirs, mud volcanoes and methane-derived authigenic carbonates (MDAC). MDAC, which may form pavements or mound structures, are produced as a direct result of methane supply from the subsurface to shallow sediment and the sediment-water interface (e.g. Bohrmann et al., 1998; Aloisi et al., 2000; Greinert et al. 2002; Bayon et al., 2009). There, methane is utilized by a consortium of methane-oxidizing archaea and sulfate-reducing bacteria in the anaerobic oxidation of methane (AOM) reaction (Hinrichs et al. 1999; Boetius et al. 2000; Reitner et al. 2005) according to Equation 1:

$$CH_{4(g)} + SO_4^{2-}{}_{(aq)} \rightarrow HCO_3^{-}{}_{(aq)} + HS^{-}{}_{(aq)} + H_2O_{(l)}$$

Eqn. 1

The reaction is maintained in expense of marine sulfate dissolved in pore waters (Boetius et al., 2000; Tsunogai et al. 2002; Niemann et al., 2005). If the supply of methane is sufficient, AOM leads to supersaturation of pore fluids with respect to HCO_3^- and in result facilitates the formation of MDAC (Hovland et al., 1987; Stakes et al. 1999; Greinert et al., 2001; Mazzini et al., 2005; Naehr et al., 2007; Paull et al., 2007; Feng et al., 2008). HS^- is typically precipitated as pyrite (FeS_2) on reaction with Fe in pore fluids (e.g. Peckmann et al., 2001; Pechmann and Thiel, 2004). Recent evidence indicates that the bacterial partners involved in AOM may be more diverse than previously thought (Beal et al., 2009) and that ANME may be able to perform

AOM without bacterial partners (Milucka et al., 2012). AOM is responsible for the oxidation of possibly 90% of marine methane (Knittel and Boetius, 2009) and hence AOM and MDAC formation are important for regulation of ocean to atmosphere carbon fluxes (e.g. Aloisi et al., 2002). Methane consumption via AOM is estimated to be in the range of 5 to 20% of net modern atmospheric methane flux (20 to 100 $x10^{12}$ g a^{-1}) (Valentine and Reeburgh, 2000). Many sites of active methane seepage have been shown to support unique macro- and micro-faunal biodiversity (e.g. Dando et al., 1991; Jensen et al., 1992; Sibuet and Olu 1998; Van Dover et al., 2003; Olu-Le Roy et al., 2004). In addition, gas seepage features are important in relation to marine industrial and petroleum safety (Hovland et al., 2002), and also in petroleum and gas prospecting (Judd and Hovland, 2007).

Most cold seeps with extensive MDAC have been reported from the deep sea (e.g. Ritger et al., 1987; von Rad et al., 1996; Chen et al., 2005; Feng et al., 2010; Haas et al., 2010; Crémière et al., 2012; Magalhães et al., 2012), but reports of extensive MDAC occurrence within the photic zone (0 to ~200 m water depth) are also common. Shallow cold seep settings with extensive MDAC occurrence include the Coal Oil Point Seep field, off Santa Barbara (Kinnaman et al., 2010), St. Lawrence Estuary, Canada (Lavoie et al., 2010), Monterey Bay (Stakes et al., 1999), the Kattegat (Jørgensen et al., 1989; Jensen et al., 1992), the Adriatic (Capozzi et al., 2012), the northwestern Black Sea (Peckmann et al., 2001), the North Sea (Hovland and Judd, 1988), and recently the Texel 11 and Holden's Reef sites in the Irish Sea (Judd et al., 2007). Shallow water seep assemblages contain lower percentage of seep specialists than deep water sites and are instead dominated by background fauna (Levin et al. 2000, Rathburn et al. 2000, Dando 2010), probably due to the increased influence and input of photosynthetic carbon in shallow depths (Levin, 2005). In

121 contrast to deep water sites, which can support abundant assemblages of seep-
122 restricted chemosymbiotic macrofauna, most symbiont-bearing taxa found in shallow
123 water sites are shared with non-seep reducing environments (Sahling et al. 2003).

124 Twenty-three mounds features have recently been identified along the Codling
125 Fault Zone (CFZ) in the east perimeter of the Kish Bank Basin in the western Irish
126 Sea (Fig. 1)(Croker et al., 2002, 2005, Judd et al., 2007). Based on extensive mapping
127 and ground-truthing, Croker et al. (2002, 2005) concluded that the mounds at the CFZ
128 were MDAC and that this site is the most active site of gas seepage in the Irish
129 designated zone of the Irish Sea. A number of the CFZ mounds were investigated in
130 2010 during INFOMAR (Integrated Mapping for the Sustainable Development of
131 Ireland's Marine Re) survey CV10_28. The purpose of this study was to further
132 ground-truth the CFZ carbonate mound features, to provide further mineralogical,
133 geochemical and isotopic evidence that these features are formed by AOM, to provide
134 evidence of current active seepage, and finally to compare this site to other extensive
135 MDAC occurrences in shallow and deep sea settings.

136

137 ## 2. Environmental and geological setting

138 The western Irish Sea (west of 5°20') encompasses two Mesozoic sedimentary basins,
139 namely the Kish Bank Basin and the southwest section of the Central Irish Basin, and
140 is primarily underlain with Permian and Carboniferous rocks. Quaternary deposits up
141 to 150 m thick occur, but are laterally discontinous, locally revealing exposed bedrock
142 (Croker et al., 2005). The northwest Irish Sea (north of 53°30') is characterised by
143 relatively weak hydrodynamic conditions, resulting in the seabed being dominated by
144 fine silty mud. This is in contrast to the southern region where the CFZ is located.
145 This region is subject to comparatively high-energy currents and is characterised by

146 gravelly sands and cobbles, and high-energy bedforms such as sand streaks, sand
147 ribbons, gravel furrows and sand waves (Croker et al., 2005). The water depth here is
148 50 to 60 m at the west of the fault and 80 to 120 m to its east. The CFZ is a major
149 northwest-southeast trending strike-slip fault and consists of a complex fault zone
150 several kilometers wide (Jackson et al., 1995). Croker et al. (2005) divided the fault
151 into three zones: the northern muddy zone containing the Lambay Deep and its
152 associated mud diapir; the central sandy zone characterised by large sand waves; and
153 the southern zone characterised by current-swept seabed and patches of coarse
154 sediments. The CFZ mounds have been identified in the central zone and have a relief
155 of 5 to 10 m. They are typically greater than 250 m in length and over 80 m in width.
156 For a detailed discussion of the setting and geology of the study area see Dobson and
157 Whittington (1979) and Jackson et al. (1995).
158

159 ## 3. Materials and Methods

160 Bathymetry data was collected from the CFZ from 2001 to 2002 during Celtic
161 Voyager survey (Croker and O'Loughlin, 2001) and available through the INFOMAR
162 program. Data was collected using a Kongsberg Simrad EM1002 multibeam
163 echosounder (see Croker and O'Loughlin, 2001, for details). During survey CV10_28
164 water column echofacies were monitored using a Kongsberg Simrad EA400 single
165 beam echosounder operated at 38 kHz. A Kongsberg Simrad OE14-208 underwater
166 towed video system, housed in a Seatronics frame was used to obtain video and image
167 stills of the mound features and surrounding seabed. Sediment sampling was
168 conducted using Shipek and Van Veen grabs. Hardground material was retrieved from
169 three stations, G103, G107 and G109, as shown in Fig. 1. Hardgrounds at each station
170 were combined as one sample per station. Details for the sampling stations are given

171 in Table 1. Samples for geochemical analysis were stored at -20°C onboard and at -
172 80°C in the laboratory. The redox potential (E_h) of sampled sediments was assessed
173 using an ORP ProcessProbe Ag/Cl redox probe (Bradley James Corp., Bedford, UK).
174 Unoriented rock slabs from G109 were cut using a diamond rock cutter and
175 polished with sandpaper. Some polished slabs were used to prepare uncovered
176 petrographic thin sections of standard size (48 mm x 28mm). Optical petrographic
177 microscopy was performed using Leica DC 300 digital camera mounted on Leica
178 DMLP microscope under the magnifications of 2.5, 5, 10, 20 and 40x. Relative
179 abundances of grains in relation to pore space were estimated using comparison charts
180 (Bacelle and Bosellini, 1965). Finely ground, hand-drilled carbonate samples from
181 G109 were analysed for stable $\delta^{13}C$ and $\delta^{18}O$ isotope ratios using Finnigan MAT 251
182 and MAT 253 mass spectrometers coupled to automated Kiel devices. $\delta^{13}C$
183 measurement of methane from sediment samples to headspace vials from a core
184 catcher was performed on a Finnegan MAT DeltaPlus irMS after conversion to CO_2
185 (Organic Mass Spectromety Facility, Woods Hole Oceanographic Institute). Isotope
186 results are measured in relation to standard VPDB, with long-term analytical precision
187 around 0.05% for $\delta^{13}C$ and 0.1% for $\delta^{18}O$.
188 Standard X-ray diffraction (XRD) in order to identify primary minerals was
189 performed on mortar-ground samples using Siemens D5005 powder X-ray
190 diffractometer. Scanning electron microscopy was performed using a Hitachi S3400-
191 N scanning electron microscopy operated at an accelerating voltage of 15.0 kV and a
192 working distance of 10 cm. Elemental composition was assessed using an INCA
193 Energy energy dispersive spectrometer (Oxford Instruments, UK) fitted to a Hitachi
194 SU-70 SEM. SEM-energy dispersive spectroscopy (EDS) was performed at an

accelerating voltage of 15.0 kV and a working distance of 1.6 cm. Elemental data was processed with the INCA suite software.

Sampled hardgrounds were acid solubilised (2 M HCl) and extracted according to Niemann et al. (2005) by ultrasonication-assisted extraction with the following solvent regime: 2:1 (v/v) methanol/DCM (x2), 1:2 (v/v) methanol/DCM (x2) and DCM (x2). Total lipid extracts were saponified with 6% KOH in methanol (80°C for 3 hr) and neutral lipids and fatty acids (at ~ pH 1) were recovered by liquid-liquid extraction (x3) with 9:1 (v/v) hexane/diethyl ether. Neutral lipids were derivatised with N,O- bis(trimethylsilyl) trifluoroacetamide/pyridine (9:1, v/v), while fatty acids were methylated with 14% BF_3 in methanol at 70°C for 1 hr. Fatty acid methyl ester (FAME) monounsaturation position was confirmed by formation of dimethyl disulfide (DMDS) adducts as outlined by Nichols et al. (1986). Analysis was performed on an Agilent 6890N gas chromatograph interfaced with an Agilent 5975C mass selective detector. The column temperature program was as follows: 65°C injection and hold for 2 min, ramp at 6°C min^{-1} to 300°C, followed by isothermal hold at 300°C for 20 min. Quantification was performed using 5-α-cholestane internal standard. Samples were analysed in duplicate by continuous flow isotope ratio mass spectrometry (IsoPrime) using identical GC conditions as above. $\delta^{13}C$ values were calibrated against a stable isotope reference standard comprising a mixture of 15 *n*-alkanes (Mixture B2, Indiana University). Average $\delta^{13}C$ values are reported after correction for addition of derivative groups where necessary. Fatty acid nomenclature is according to $xC_{y\omega z}$, where *x* refers to the number of carbon atoms present, *y* refers to the number of double bonds on the carbon chain and *z* refers to the position of the first double bond from the methyl end.

220 # 4. Results

221 ## 4.1 Underwater towed video, sampling and single beam echosounder

222 Collected video and image stills of the seabed at and in the vicinity of the mound
223 targets are presented in Fig. 2. The sediment type was primarily fine- to coarse-
224 grained sand, and there was widespread occurrence of exposed and semi-exposed
225 hardgrounds on the seabed in the vicinity of target sites (Fig. 2A and B). These
226 features appeared to be largely buried by sand. Fig. 2C shows an underwater still
227 image of an area of exposed stacked pavement. This shows large 10 to 20 cm thick
228 slabs and likely represents the characteristic morphology of the CFZ mounds. Patches
229 of black, apparently reduced seabed several centimetres across were also recorded
230 (Fig. 2D and F) during video surveying. A high density of asterozoans (likely
231 ophiuroids) was observed in the vicinity of the mounds (not shown). In addition,
232 possible hydroids colonising hardgrounds were also recorded (Fig. 2D to F).

233 Grab sampling of stations G103, G107 and G109 retrieved hardground
234 material (hereafter referred to as G103, G107 or G109) and some black sediment.
235 Sampled black surface sediments (Fig. 2G and I) were confirmed to be reducing,
236 exhibiting E_h readings as low as -177 mV. Colonising hydroids were also retrieved,
237 still physically attached to sampled hardgrounds (Fig. 2G and H). These possibly
238 belong to the genus *Nemertesia*, which have been found at the Texel carbonate mound
239 sites (~ 53°27'N, 5°12'W) in the mid-Irish Sea (Whomersley et al., 2010). Grab
240 sampling stations G103, G107 and G109 contained cemented tube worms (Fig. 2G).
241 These are likely to have been formed by sedentary sabellarid polychaetes, possibly
242 *Sabellaria spinulosa*, which are abundant at other hard grounds in the Irish Sea
243 (Whomersley et al., 2010).

Single beam echosounder transects across one of the mounds (Fig. 1B) yielded characteristic acoustic echofacies in the water column. These appear as a rising vertical plume from close to the apex of the mound (Fig. 3). This acoustic signal is either caused by fish shoals or gas bubbles. However, fish shoals would normally display a broader more horizontal profile (Judd and Hovland, 2007), and by virtue of the source and vertical profiles this is very likely a gas plume emanating from the mound. The plume was detected rising a number of metres into the water column and the profile indicates at least moderate seepage is taking place at the CFZ.

4.2 Mineralogy, petrographic analysis and stable isotope analysis

Sub-samples from G103, G107 and G109 were also analysed using SEM-EDS analysis (Fig. 4). EDS spectra were dominated by calcium, silica, carbon and oxygen, confirming that the hard grounds are composed of carbonate and carbonate-cemented quartz grains (Fig. 4A and B). Individual quartz grains cemented by this carbonate are shown in Fig. 4C. Sulfur was also identified from EDS spectra, in particular for G109 (Fig. 4B). SEM micrographs highlighted the occurrence of amorphous to well-developed framboidal pyrite as the source of this sulfur (Fig. 4D and E). Based on the crystal shapes observed in SEM, the carbonate appears to a primarily acicular aragonite. Further petrographic analysis (Fig. 5, thin section PMO 217.327) and XRD (Fig. 6) of G109 confirmed that quartz and aragonite are the major mineral constituents of the rock. The rock can be subdivided into two main components. A detrital component is composed mostly of quartz sand (Fig. 5A), with small admixtures of other grains, such as mudstone lithoclasts, glaucony grains (Fig. 5B) and bioclasts. Among the bioclasts, possible red algae (Fig. 5B), echinoderms (Fig. 5B), bivalve fragments (Fig. 5C), balanid barnacles (Fig. 5D), foraminifera and

gastropods (Fig. 5E and F) have been identified. This component can be linked with quartz and magnesian calcite, as identified by XRD (Fig. 6). The total grain fabric constitutes around 60% of the rock volume. Pore space partially occluded by the authigenic component occupies the remaining 40% of rock volume. The authigenic component is composed almost solely of aragonite (Fig. 6). It is represented by the microcrystaline variety, lining the surface of some of the grains and occasionally forming clothed microfabrics, followed by more abundant acicular crystals cementing the pore space (Fig. 5).

Carbonate stable isotope data have been obtained from sites G107 and G109. The values from a single sample from site G107 are shown in Table 1. Samples from site G109 are presented in Table 1 (range) and Table 2 (all data points). Site G107 shows depleted $\delta^{13}C$ carbon (-36.97‰) and enriched $\delta^{18}O$ value (3.54‰). Site G109 shows predominantly low $\delta^{13}C$ values, concentrated around -50‰ and reaching down to -53.71‰, with only two samples showing higher values (Fig. 7). $\delta^{18}O$ varied between -0.80 and 2.58‰ (Fig. 7), with most samples exhibiting heavier values (Fig. 7). $\delta^{13}C$ values for methane sampled from surface sand at the CFZ mounds (Lat. 53°20’50”N, Long. 5°39’10”W) measured -70‰.

4.3 Lipid biomarkers and compound specific stable carbon isotope analysis

Fatty acids distribution was similar between G103, G107 and G109, whereby a range of saturated, monounsaturated, polyunsaturated, methyl- and cyclopropyl fatty acids were observed (Fig. 8A). Fatty acids ranged from C_{12} to C_{26} homologs. $C_{16:0}$ was the major fatty acid in all samples. $C_{14:0}$ and $C_{18:0}$ were other major saturated fatty acids. Monounsaturated $C_{16:1\omega7}$ and $C_{18:1\omega7}$ were also major fatty acids, followed by the polyunsaturated fatty acids $C_{20:5\omega3}$, $C_{20:4\omega6}$, $C_{22:6\omega3}$ and $C_{22:5\omega6}$. Iso and anteiso methyl

294 branched fatty acids were also abundant and were dominated by odd carbon C_{15} and
295 C_{17} homologs. These included *i*$C_{15:0}$, *ai*$C_{15:0}$, *i*$C_{16:0}$, 10Me$C_{16:0}$ and *i*$C_{17:0}$. The average
296 (n = 2) measured $\delta^{13}C$ values for selected lipids from G103, G107 and G109 are given
297 in Fig. 9. The $\delta^{13}C$ measurements for fatty acids ranged from -24‰ to as low as -
298 39‰. A general trend of between -25‰ to -29‰ was observed with overall little
299 variation between samples for each compound. However, the branched fatty acids
300 *ai*$C_{15:0}$, *i*$C_{16:0}$, 10Me$C_{16:0}$ and $C_{17:1}$ were more depleted (below -30‰) for G109, as
301 well as with *i*$C_{16:0}$ for G107. Sterols were the major lipid class in the neutral lipid
302 fractions. $C_{27}\Delta^5$ was the major sterol in all samples. $C_{26}\Delta^{5,22}$, $C_{27}\Delta^{5,22}$, $C_{28}\Delta^{5,22}$,
303 $C_{29}\Delta^{5,22}$, $C_{29}\Delta^5$ and $C_{29}\Delta^{5,24(28)}$ were also identified. $\delta^{13}C$ values were about -28‰ for
304 well-resolved major sterols (Fig. 9). Other major lipids included phytol, *n*-alkanols
305 (C_{14} to C_{26}), a range of mono-alkyl glycerol ethers (MAGE) with *n*-alkyl chain
306 lengths from C_{14} to C_{20}. Pentamethylicosane was identified in G109 in low
307 abundance, as well as crocetane co-eluting with phytane. Archaeol was tentatively
308 identified in low abundance in G103 based on the peaks at m/z 130, 278 and 426. The
309 abundance of these lipids was too low to permit $\delta^{13}C$ measurement.
310
311 **5. Discussion**
312 Methanogenesis in marine sediments can be subdivided into three main stages. The
313 first stage takes place during shallow burial, when in temperatures lower than 50°C
314 organic matter is being converted into methane by series of biochemical processes
315 (Mah et al., 1977). In later burial at 80°C to 120°C, thermal cracking of organic
316 matter forms gaseous and liquid hydrocarbons, which are further cracked to methane
317 in when temperatures reach ca. 150°C (Claypool and Kvenvolden, 1983). Each of the
318 formation stages leaves a characteristic trace in isotopic and chemical composition of

319 the resulting gas (Schoell, 1988; Whiticar, 1999), which can be used to trace back the
320 origin of the methane (e.g. Martens et al., 1991; Ivanov et al., 2010). Usually, the
321 biogenic methane is significantly depleted in the heavy carbon isotope, with $\delta^{13}C$
322 values below -50‰, with thermogenic methane ranging between -50‰ to -30‰
323 (Sackett, 1978; Peckmann and Thiel, 2004; Judd and Hovland, 2007).

324 Heavily depleted carbon isotope (as low as -53.7‰) data from hardgrounds
325 sampled at stations G107 and G109 confirm that the CFZ mounds are MDAC, and
326 support previous work from Croker et al. (2002, 2005). Along with the Texel 11 and
327 the Holden's Reef sites, the CFZ mounds are the third confirmed occurrence of
328 MDAC in the Irish Sea (Judd, 2005; Judd et al., 2007). Usually MDAC is less
329 depleted than parent gas due to mixing with carbon from other sources, so the exact
330 correlation between carbonate and parent gas is not straightforward (e.g. Bohrmann et
331 al., 1998, Peckmann et al., 2001, Schmidt et al., 2002; Peckmann and Thiel, 2004).
332 The amount of mixing is unknown, but seeping methane was likely isotopically
333 lighter than cements and hence possiblly of biogenic origin. In addition, the $\delta^{13}C$ for
334 methane recovered from surface sediment in this region measured -70‰.
335 Accumulations of unidentified shallow gas north of the study area have been
336 suggested previously to be of biogenic origin (Yuan et al., 1992). Gas generation
337 within these sediments is possible, however the volume of gas generated from thin
338 and fairly recent sediment (Belderson, 1964) is probably much lower than that
339 observed (Clayton, 1992; Judd and Hovland, 2007). Because the area of study is
340 dominated by sands (Belderson, 1964; Croker et al., 2005), the gas is most likely
341 sourced from the deeper subsurface. Subcropping Palaeozoic and Mesozoic rocks of
342 the Kish Bank Basin (Naylor et al., 1993) are obvious candidates, with Carboniferous
343 coals subjected to biogenesis to methane being of particular interest here (e.g. Flores

et al., 2008; Li et al., 2008; Ulrich and Bower, 2008; cf. Moore, 2012). Alternatively, significant mixing and microbial reworking of seeping thermogenic gas in the shallow subsurface would result in a further depleted isotope signal from the original thermogenic signature and may be occurring here. Indeed Croker et al. (2005) favoured a thermogenic gas source based on the distribution of gas accumulations in the western Irish Sea at both sandy and muddy sediment types, and due to the occurrence of most gas accumulations and features along faults (migration pathways from the deep sub-surface). Thus, the exact source of the gas remains difficult to determine at present. The interpretation of oxygen isotope values is also problematic since variation of $\delta^{18}O$ between the G107 and G109 sites suggests formation of MDAC is in disequilibrium with marine water and some influence of seeping fluids.

Active water column seepage from the CFZ mounds has been documented on one other occasion at a separate feature in the CFZ, approximately 2.5 km west (53°20’30” N, 5°39’10” S) of the site described here (Croker et al., 2002). Based on surveys to date, the CFZ appears to be a site of active gas seepage. $\delta^{13}C$ analysis has confirmed that the precipitated carbonate is MDAC and SEM-EDS and has also highlighted the presence of co-precipitated pyrite. This is in agreement with previous observations (Croker et al., 2002). Sulfate reduction is also evidenced by the presence of patches of black reducing sediments at the sediment-water interface (Fig. 2D and F). AOM is therefore a significant process regulating the flux of methane from the CFZ mounds and the formation of carbonate mounds at this site. The size and thickness of the slabs shown in Fig. 2C indicate considerable seepage over geological time, and together with echosounder data, and the presence of sulfide-rich reduced sediment indicates active methane seepage from the CFZ mounds is ongoing. Marine settings experiencing long-term erosion will eventually expose MDAC formed by

AOM and, since carbonate-cemented sediments are more resistant to erosion than uncemented sediments, exhumed MDAC will accumulate as lag deposits in erosional environments (Paull and Ussler, 2008). The CFZ is a dynamic erosional setting with strong hydrographic conditions (e.g. Gowen and Stewart, 2005), and it is likely that the mounds formed in the shallow subsurface and have become exposed over time. The topography of these features is also likely extensively eroded post-exposure.

Both the character of the detrital and authigenic component suggests carbonate authigenesis within the sediment. This seems to be a common phenomenon in most of the seeps in the marine environment (e.g. Naehr et al., 2007; Pierre and Fouquet 2007; Himmler et al., 2011), since AOM is localized to the anoxic zone at some depth within the sediment (Hinrichs et al. 1999, Boetius et al. 2000). Aragonite forms in favour over calcite in settings with relatively high alkalinity and increased sulfate concentrations (Walter, 1986; Burton, 1993). In this way, in seep settings aragonite is preferentially formed closer to the sediment-water interface (Beauchamp and Savard, 1996; Aloisi et al., 2002). Formation of authigenic carbonate proceeds downward from the initial sulfate-methane transition to form carbonate crust (Greinert et al., 2002; Bayon et al., 2009). As AOM proceeds, marine sulfate enclosed in the pore water is successively consumed, giving way for more extensive precipitation of calcite in the succeeding stages (e.g. Aloisi et al., 2002; Bayon et al., 2009). Dominance of aragonite over calcite in carbonates sampled (Fig. 6) implies their formation in a sulfate-rich environment, most likely shaped by seawater reflux through permeable sandy sediment (Fig. 5).

Nemertesia and *Sabellaria* are epifaunal animals, which require a solid substrate for colonisation (Whomersley et al., 2010). *Sabellaria spinulosa* favours a sandy erosional environment but requires a hard ground in order to get established.

394 This species was found in very high densities covering MDAC in the mid-Irish Sea
395 (Whomersley et al., 2010) and may be an important coloniser of carbonate grounds
396 throughout the Irish Sea. No known seep-specialist macrofauna, such as siboglinid
397 tubeworms or thyasirid bivalves (Dando et al., 1991) were observed during video
398 surveying. Nor were bacterial mats, which are commonly reported in active methane
399 seep environments (e.g. Niemann et al. 2005, Bouloubassi et al. 2009). Seep-
400 specialists such as some siboglinid tubeworms are rarely reported in shallow shelf and
401 coastal cold seeps and are largely restricted to deep-sea active cold seep settings (Judd
402 and Hovland 2007). Thus they would not be expected to occur in a setting such as the
403 CFZ seeps. However, a more comprehensive survey of the macrofaunal diversity of
404 the mounds is needed to rule out the occurrence and activity of seep-specialists at the
405 CFZ. It is evident that these hard grounds are of importance as a solid substrate for
406 normal marine epifauna, allowing for diverse ecosystems to develop (Whomersley et
407 al., 2010), as has been observed in the North Sea (Dando et al., 1991; Jensen et al.,
408 1992).

409 The CFZ seep carbonates contain major fatty acids previously reported among
410 sulfate-reducing bacteria implicated in AOM (Aloisi et al., 2002; Elvert et al., 2003;
411 Niemann and Elvert 2008). These included *i*$C_{15:0}$, *ai*$C_{15:0}$, $C_{16:1\omega5c}$, $C_{17:1\omega6c}$ and
412 cyc$C_{17:0}$ (Fig. 8A). *ai*$C_{15:0}$, *i*$C_{16:0}$ and $C_{17:1}$ fatty acids, in particular for G109 (and
413 *i*$C_{16:0}$ for G107) were more depleted than other fatty acids, which suggests that
414 sulfate-reducing bacteria involved in AOM are present. However, in general measured
415 $\delta^{13}C$ values for most fatty acids were not significantly depleted in ^{13}C (Fig. 9) and
416 suggests that methane is not a primary substrate for the dominant bacterial
417 populations in this setting, as has been found in some other active seep settings (e.g.
418 Pancost et al., 2000; Elvert et al., 2003, Niemann et al., 2005). MAGE have

419 previously been reported as diagnostic lipids for sulfate-reducing bacteria implicated
420 in AOM (Pancost et al., 2001; Rütters et al., 2001). However, $\delta^{13}C$ measurements
421 indicate that water column input is the major source of MAGE in this study (Fig. 9).
422 This conclusion is supported by the widespread occurrence of MAGE in sediments
423 and in the water column in the western Irish Sea (unpublished data).

424 Commonly reported archaeal lipids such as crocetane (co-eluting with
425 phytane), pentamethyleicosane and archaeol were observed, but in low abundance
426 (Fig. 8B). This indicates archaea are a minor contributor to overall organic matter
427 within these hardgrounds. These lipids are frequently among the most abundant and
428 ^{13}C-depleted at active methane seeps (Pancost et al., 2000; Aloisi et al., 2002;
429 Niemann et al., 2005; Bouloubassi et al., 2009). In this case biomarkers diagnostic for
430 microalgal water column input, such as sterols, phytol and C_{14} to C_{22} *n*-alkanols
431 (Volkman, 2006) were dominant in all samples. This suggests that water column input
432 derived from marine plankton, as well as benthic microalgae, is the dominant organic
433 matter signal in the cemented sands. Considering that the CFZ zone is located in
434 shallow shelf waters in a setting of known high primary productivity (Gowen and
435 Stewart, 2005), a dominant input of organic matter from the water column may be
436 expected. $\delta^{13}C$ values therefore likely reflect this major input from photosynthetic and
437 related heterotrophic processes and may be diluting signals from microbial biomass
438 that could be incorporating methane (Aquilina et al., 2010). It is noteworthy, however,
439 that certain bacterial fatty acids were more depleted relative to other lipids and
440 measured values were as low as -40‰ (Fig. 9), which suggests that an unknown
441 proportion of these fatty acids may be associated with sulfate-reducing bacteria
442 involved in AOM. Similar moderately depleted fatty acids diagnostic for sulfate-
443 reducing bacteria were obtained by Kinnaman et al. (2010) from MDAC concretions

444 at 10 m water depth in the Brian Seep off Santa Barbara. AOM consortium biomass
445 and their associated lipids are spatially highly variable and typically is highest in
446 defined locales below the sediment surface where AOM rates are highest (e.g. Elvert
447 et al., 2005; Aquilina et al., 2010). Therefore further targeted surveys in proximity to
448 a venting site and from subsurface MDAC may reveal the nature of the
449 microorganisms involved in AOM at this setting. This study highlights the complex
450 interplay at shallow active gas seeps, between microbes utilising carbon derived from
451 marine photosynthesis, and carbon from seeping gas.
452

453 ## 6. Conclusions

454 Bulk isotope analysis and mineralogical analysis has confirmed that the carbonate
455 mound features at the CFZ in the Irish Sea are MDAC, similar to the Holden's Reef
456 and the Texel 11 sites. The principal authigenic mineral is aragonite. Active seepage
457 was recorded from one of the mounds, with gas plumes detected in the water column.
458 Underwater video footage highlighted the presence of sand-covered stacked and
459 exposed carbonate pavements. The occurrences of high densities of cemented
460 sabellarid tubes and extensive macrofaunal colonisation of carbonates indicate the
461 CFZ mounds, like at other MDAC sites in the Irish Sea, represent an important solid
462 substrate and habitat for local macrofauna. The common occurrence of patches of
463 reduced sediment and the association of authigenic aragonite with framboidal pyrite
464 indicate that AOM is taking place in shallow subsurface. In contrast to other deep sea
465 methane seeps with widespread MDAC, lipid biomarker analysis suggests that
466 microbial organic matter derived from methane is of minor significance in
467 comparison to algal detrital organic matter from the water column. The co-existence
468 of $\delta^{13}C$–depleted authigenic aragonite and isotopically light methane indicates a

469 biogenic origin of the seeping gas, possibly related to Carboniferous coal deposits.
470 However microbial reworking of deep thermogenic methane cannot be ruled out at
471 present.
472
473

474 Acknowledgements

475 We thank the crew of the RV Voyager for their help and patience and the INtegrated
476 Mapping FOr the Sustainable Development of Ireland's MARine Resource
477 (INFOMAR), the Irish Shelf Petroleum Studies Group of the Petroleum Infrastructure
478 Programme, the Irish Environmental Protection Agency (EPA), QUESTOR (Queens
479 University Belfast), the Irish Council for Science, Engineering & Technology
480 (IRCSET), the Geological Survey of Ireland (GSI) and the Science foundation of
481 Ireland (SFI) for funding this research
482

483 References

484 Aloisi, G., Pierre, C., Rouchy, J.-P., Foucher, J.-P., Woodside, J. and the MEDINAUT
485 Scientific Party. 2000. Methane-related authigenic carbonates of eastern Mediterranea
486 Sea mud volcanoes and their possible relation to gas hydrate destabilization. Earth
487 and Planetary Science Letters 184, 321-338.

488 Aloisi, G., Bouloubassi I., Heijs S.K., Pancost R.D., Pierre C., Sinninghe Damsté J.S.,
489 Gottschal J.C., Forney, L.J. 2002. CH_4-consuming microorganisms and the formation
490 of carbonate crusts at cold seeps. Earth and Planetary Science Letters 203, 195-
491 203.

492 Bacelle, L., Bosellini, A. 1965. Diagrammi per la stima visiva della composizione
493 percentuale nelle rocce sedimentarie. Annali della Universitá di Ferrara, Sezione IX,
494 Science Geologiche e Paleontologiche 1:59-62.
495 Bayon, G., Henderson, G.M., Bohn, M. 2009. U-Th stratigraphy of a cold seep
496 carbonate crust. Chemical Geology 260, 47-56.
497 Belderson, R.H. 1964. Holocene sedimentation in the western half of the Irish Sea.
498 Marine Geology 2,147-163.
499 Beal E.J., House C.H., Orphan V.J. 2009. Manganese-and iron-dependent marine
500 methane oxidation. Science 325, 184-187.
501 Boetius, A., Ravenschlag, K., Schubert, C.J., Rickert, D., Widdel, F., Gieseke, A.,
502 Amann, R., Jørgensen, B.B., Witte, U., Pfannkuche, O. 2000. A marine microbial
503 consortium apparently mediating anaerobic oxidation of methane. Nature 407,
504 623-626.
505 Boetius, A., Suess, E. 2004. Hydrate Ridge: a natural laboratory for the study of
506 microbial life fueled by methane from near-surface gas hydrates. Chemical Geology
507 2005, 291-310.
508 Bohrmann, G., Greinert, J., Suess, E., Torres, M. 1998. Authigenic carbonates from
509 the Cascadia subduction zone and their relation to gas hydrate stability. Geology 26,
510 647-650.
511 Bouloubassi, I., Nabais, E., Pancost, R.D., Lorre, A., Taphanel, M.H. 2009. First
512 biomarker evidence for methane oxidation at cold seeps in the Southeast Atlantic
513 (REGAB pockmark). Deep Sea Research Part II: Topical Studies in Oceanography
514 56, 2239-2247.
515 Burton, E.A. 1993. Controls on marine carbonate cement mineralogy: review and

516 reassessment. Chemical Geology 105, 163–179.

517 Capozzi, R., Guido, F.L., Oppo, D., Gabbianelli, G. 2012. Methane-Derived
518 Authigenic Carbonates (MDAC) in northern-central Adriatic Sea: Relationships
519 between reservoir and methane seepages. Marine Geology 332-334, 174-188.

520 Chen, D.F., Huang, Y.Y., Yuan, X.L., Cathles III, L. M. 2005 Seep carbonates and
521 preserved methane oxidizing archaea and sulfate reducing bacteria fossils suggest
522 recent gas venting on the seafloor in the Northeastern South China Sea. Marine and
523 Petroleum Geology 22, 613-621

524 Claypool, G.E., Kvenvolden, K.A. 1983. Methane and other hydrocarbon gases in
525 marine sediment. Annual Review of Earth Sciences 11, 299-327.

526 Clayton, C. 1992. Source volumetrics of biogenic gas generation, in: Vially, R. (Ed.)
527 Bacterial Gas. Paris, Editions Technip, 191-204.

528 Crémière, A., Pierre, C., Blanc-Valleron, M.-M., Zitter, S., Çağatay, M.N., Henry, P.
529 2012. Methane-derived authigenic carbonates along the North Anatolian fault system
530 in the Sea of Marmara (Turkey). Deep-Sea Research I 66, 114-130

531 Croker, P.F. 1995. Shallow gas accumulation and migration in the western Irish Sea.
532 Geological Society of London, Special Publications 93, 41-58.

533 Croker, P.F., O'Loughlin, O. 2001. Celtic Voyager Cruise Report – 18th - 19th April,
534 4th - 6th May. Petroleum Affairs Division, Dublin, December 2001

535 Croker, P.F., Garcia-Gil, S., Monteys, X., O'Loughlin, O. 2002. A multibeam survey
536 of the Codling Fault Zone, western Irish Sea. Irish Geological Research Meeting,
537 UCD, Ferbuary 2002.

538 Croker, P.F., Kozachenko, M., Wheeler, A.J. 2005. Gas-related seepage features in
539 the western Irish Sea IRL-SEA6. Tech Rep Strategic Environmental Assessment of

the Irish Sea (SEA6). Petroleum Affairs Division: Dublin, Ireland.

Dando, P. 2010. Biological Communities at Marine Shallow-Water Vent and Seep Sites, in: Kiel, S. (Ed.). Vent and Seep Biota. Aspects from Microbes to Ecosystems, Dodrecht, Heidelberg, London, New York, Springer, p. 333-378.

Dando, P., Austen, M., Burke, R., Kendall, M., Kennicutt, M., Judd, A., Moore, D.C., O'Hara, S.C.M., Schmaljohann, R., Southward, A.J. 1991. Ecology of a North Sea pockmark with an active methane seep. Marine Ecology Progress Series 70, 49-63

Dobson, M., Whittington, R. 1979. The geology of the Kish Bank Basin. Journal Geological Society London 136, 243-249.

Elvert, M., Boetius, A., Knittel, K., Jørgensen, B.B. 2003. Characterization of specific membrane fatty acids as chemotaxonomic markers for sulfate-reducing bacteria involved in anaerobic oxidation of methane. Geomicrobiology Journal 20, 403-419.

Feng, D., Chen, D., Roberts, H.H. 2008. Sedimentary fabrics in the authigenic carbonates from Bush Hill: implication for seabed fluid flow and its dynamic signature. Geofluids 8, 301-310.

Feng, D., Chen, D., Peckmann, J., Bohrmann, G. 2010. Authigenic carbonates from methane seeps of the northern Congo fan: Microbial formation mechanism. Marine and Petroleum Geology 27, 748-756.

Fleischer, P., Orsi, T., Richardson, M., Anderson, A. 2001. Distribution of free gas in marine sediments: a global overview. Geo-Marine Letters 21, 103-122.

Flores, R.M., Rice, C.A., Stricker, G.D., Warden, A., Ellis, M.S. 2008. Methanogenic pathways of coal-bed gas in the Powder River Basin, United States: The geologic factor. International Journal of Coal Geology 27, 52-75.

563 Flügel, E. 2004. Microfacies of carbonate rocks. Analysis, Interpretation and
564 Application. Springer Verlag, Berlin Heidelberg, 976 pp.
565 Forster, P., Ramaswamy, V., Artaxo P., Berntsen, T., Betts, R., Fahey, D.W.,
566 Haywood, J., Lean, J., Lowe, D.C., Myhre, G., Nganga, J., Prinn, R., Raga, G.,
567 Schulz, M., Van Dorland, R. 2007. Changes in atmospheric constituents and in
568 radiative forcing, in: Solomon, S., Qin, D., Manning, M., Chen, Z., Marquis, M.,
569 Averyt, K.B., Tignor, M., Miller, H.L. (Eds.). Climate Change 2007: The physical
570 science basis. Contribution of Working Group I to the Fourth Assessment Report of
571 the Intergovernmental Panel on Climate Change, Cambridge, Cambridge University
572 Press: United Kingdom and USA, p. 129-234.
573 Friedman, G.M. 1959. Identification of carbonate minerals by staining methods.
574 Journal of Sedimentary Petrology 29, 87-97.
575 Gowen R.J., Stewart B. 2005. The Irish Sea: nutrient status and phytoplankton.
576 Journal of Sea Research 54, 36-50.
577 Greinert, J., Bohrmann, G., Suess, E. 2001: Gas hydrate-associated carbonates and
578 methane-venting at Hydrate Ridge: Classification, distribution and origin of
579 authigenic lithologies, in: Paull, C.K., Dillon, P.W. (Eds.), Natural Gas Hydrates:
580 Occurrence, Distribution and Detection. Geophysical Monograph 124, 99-113.
581 Greinert, J., Bohrmann, G., Elvert, M. 2002. Stromatolitic fabric of authigenic
582 carbonate crusts: result of anaerobic methane oxidation at cold seeps in 4,850 m water
583 depth. Interational Journal Of Earth Sciences 91, 698-711.
584 Haas A., Peckmann, J., Elvert, M., Sahling, H., Bohrmann, G. 2010. Patterns of
585 carbonate authigenesis at the Kouilou pockmarks on the Congo deep-sea fan. Marine
586 Geology 268, 129-136.

587 Himmler, T., Brinkmann, F., Bohrmann, G., Peckmann, J. 2011. Corrosion patterns of
588 seep-carbonates from the eastern Mediterranean Sea. Terra Nova 23, 206-212
589 Hinrichs, K.-U., Hayes, J.M., Sylva, S.P., Brewer, P.G. DeLong, E.F. 1999. Methane-
590 consuming archaebacteria in marine sediments. Nature 398, 802-805.
591 Hovland, M., Talbot, M.R., Qvale, H., Olaussen, S., Aasberg, L. 1987. Methane-
592 related carbonate cements in pockmarks of the North Sea. Journal of Sedimentary
593 Petrology 57, 881-892.
594 Hovland, M., Gardner, J., Judd, A. 2002. The significance of pockmarks to
595 understanding fluid flow processes and geohazards. Geofluids 2, 127-136.
596 Hovland, M., Svensen, H., Forsberg, C.F., Johansen, H., Fichler, C., Fosså, J.H.,
597 Jonsson, R., Rueslåtten, H. 2005. Complex pockmarks with carbonate-ridges off mid-
598 Norway: Products of sediment degassing. Marine Geology 218, 191-206.
599 Ivanov, M., Mazzini, A., Blinova, V., Kozlova, E., Laberg. J.-S., Matveeva, T.,
600 Taviani, M., Kaskov, N. 2010. Seep mounds on the Southern Vøring Plateau. Marine
601 and Petroleum Geology 27, 1235-1261.
602 Jackson, D.I., Jackson, A.A., Evans, D., Wingfield, R.T.R., Barnes, R.P., Arthur, M.J.
603 1995. The geology of the Irish Sea. BGS UK Offshore regional Rep, HMSO, London.
604 Jensen, P., Aagaard, I., Burke, Jr R.A., Dando, P.R., Jørgensen, N.O., Kuijpers, A.,
605 Laier, T., O'Hara, S.C.M., Schmaljohann, R. 1992. 'Bubbling reefs in the Kattegat:
606 Submarine landscapes of carbonate-cemented rocks support a diverse ecosystem at
607 methane seeps. Marine Ecology Progress Series 83, 103-112.
608 Levin, L.A., James, D.W., Martin, C.M., Rathburn, A.E., Harris, L.H., Michener,
609 R.H. 2000. Do methane seeps support distinct macrofaunal assemblages?
610 Observations on community structure and nutrition from the northern California slope

611 and shelf. Marine Ecology Progress Series 208, 21-39.

612 Levin, L.A. 2005. Ecology of cold seep sediments: interactions of fauna with flow,
613 chemistry and microbes, in: Gibson, R.N., Atkinson, R.J.A., Gordon, A.G.M. (Eds.).
614 Oceanography and Marine Biology: An Annual Review 43, 1-46.

615 Jones, G.B., Floodgate, G., Bennell, J. 1986. Chemical and microbiological aspects of
616 acoustically turbid sediments: preliminary investigations. Marine Georesources and
617 Geotechnology 6, 315-332.

618 Jørgensen, N.O. 1989. Holocene methane-derived dolomite-cemented sandstone
619 pillars from the Kattegat, Denmark. Marine Geology 88, 71-81.

620 Judd, A., Croker, P., Tizzard, L., Voisey, C. 2007. Extensive methane-derived
621 authigenic carbonates in the Irish Sea. Geo-Marine Letters 27, 259-267.

622 Judd, A., Hovland, M. 2007. Seabed fluid flow: the impact on geology, biology and
623 the marine environment. Cambridge University Press: Cambridge, UK.

624 Judd, A.G. 2005. Strategic Environmental Assessment of the Irish Sea (SEA6): The
625 distribution and extent of methane-derived authigenic carbonate. Department of Trade
626 and Industry, United Kingdom.

627 Kinnaman, F.S., Kimball, J.B., Busso, L., Birgel, D., Ding, H., Hinrichs, K.-U.,
628 Valentine, D.L. 2010. Gas flux and carbonate occurrence at a shallow seep

629 of thermogenic natural gas. Geo-Marine Letters 30, 355-365.

630 Knittel, K., Boetius, A. 2009. Anaerobic oxidation of methane: progress with an
631 unknown process. Annual Reviews of Microbiology 63, 311-334.

632 Lavoie, D., Pinet, N., Duchesne, M., Bolduc, A., Larocque, R. 2010. Methane-derived
633 authigenic carbonates from active hydrocarbon seeps of the St. Lawrence Estuary,
634 Canada. Marine and Petroleum Geology 27, 1267-1272.

635 Levin, L.A. 2005. Ecology of cold seep sediments: interactions of fauna with flow,
636 chemistry and microbes. Oceanography and Marine Biology: An annual Review 43,
637 1-46.
638 Li, D., Hendry, P., Faiz, M. 2008. A survey of the microbial populations in some
639 Australian coalbed methane reservoirs. International Journal of Coal Geology 27, 14-
640 24.
641 Little, C.T.S., Campbell, K.A., Herrington, R.J. 2002. Why did ancient
642 chemosynthetic seep and vent assemblages occur in shallower water than they do
643 today? Comment. International Journal of Geosciences 91, 149-153.
644 Mah, R.A., Ward, D.M., Baresi, L., Glass, T.L. 1977. Biogenesis of methane. Annual
645 Review of Microbiology 31, 309-341.
646 Magalhães, V.H., Pinheiro, L.M., Ivanov, M.K., Kozlova, E., Blinova, V., Kolganova,
647 J., Vasconcelos, C., McKenzie, J.A., Bernasconi, Kopf, A.J., Díaz-del-Río, V.,
648 González, F.J., Somoza, L. 2012. Formation processes of methane-derived authigenic
649 carbonates from the Gulf of Cadiz. Sedimentary Geology 243-244, 155-168.
650 Martens, C.S., Chanton, J.P., Paull, C.K. 1991. Biogenic methane from abyssal brine
651 seeps at the base of the Florida escarpment. Geology 19, 851-854.
652 Mazzini, A., Aloisi, G., Akhmanov, G.G., Parnell, J., Cronin, B.T., Murphy, P. 2005.
653 Integrated petrographic and geochemical record of hydrocarbon seepage on the
654 Vøring Plateau. Journal of the Geological Society 162, 815-827.
655 Milucka, J., Ferdelman, T.G., Polerecky, L., Franzke, D., Wegener, G., Schmid, M.,
656 Lieberwirth, I., Wagner, M., Widdel, F., Kuypers, M.M. 2012. Zero-valent sulphur is
657 a key intermediate in marine methane oxidation. Nature 491,541-546.
658 Moore, T.A. 2012. Coalbed methane: A review. International Journal of Coal
659 Geology 101, 36-81.

660 Mount, J. 1985. Mixed siliciclastic and carbonate sediments: a proposed first-order
661 textural and compositional classification. Sedimentology 32, 435-442.
662 Naehr, T.H., Eichhubl, P., Orphan, V.J., Hovland, M., Paull, C.K., Ussler III, W.,
663 Lorenson, T.D. & Greene, H.G. 2007. Authigenic carbonate formation at hydrocarbon
664 seeps in continental margin sediments: a comparative study. Deep-Sea Research II,
665 54, 1268-1291.
666 Naylor, D., Haughey, N., Clayton, G. & Graham, J.R. 1993. The Kish Bank Basin,
667 offshore Ireland, in: Parker, J.R. (Ed.). Petroleum Geology of Northwest Europe:
668 Proceedings of the 4th Conference. Petroleum Geology Conference series 4, 845-855.
669 Nichols, P.D., Guckert, J.B., White, D.C. 1986. Determination of monosaturated fatty
670 acid double-bond position and geometry for microbial monocultures and complex
671 consortia by capillary GC-MS of their dimethyl disulphide adducts. Journal of
672 Microbiological Methods 5:49-55.
673 Niemann, H., Elvert, M. 2008. Diagnostic lipid biomarker and stable carbon isotope
674 signatures of microbial communities mediating the anaerobic oxidation of methane
675 with sulphate. Organic Geochemistry 39, 1668-1677.
676 Niemann, H., Elvert, M., Hovland, M., Orcutt, B., Judd, A., Suck, I., Gutt, J., Joye, S.,
677 Damm, E., Finster, K., Boetius, A. 2005. Methane emission and consumption at a
678 North Sea gas seep (Tommeliten area). Biogeosciences Discussions 2, 1197-1241.
679 Olu-Le Roy, K., Sibuet, M., Fiala-Medioni, A., Gofas, S., Salas, C., Mariotti, A.,
680 Foucher, J.P. Woodside, J. 2004: Cold seep communities in the deep eastern
681 Mediterranean Sea: composition, symbiosis and spatial distribution on mud
682 volcanoes. Deep-Sea Research I 51, 1915-1936.
683 Pancost, R.D., Bouloubassi, I., Aloisi, G., Sinninghe Damsté, J.S. 2001. Three series

684 of non-isoprenoidal dialkyl glycerol diethers in cold-seep carbonate crusts. Organic
685 Geochemistry 32, 695-707.

686 Pancost, R.D., Sinninghe Damste, J.S., de Lint, S., van der Maarel, M.J., Gottschal,
687 J.C. 2000. Biomarker evidence for widespread anaerobic methane oxidation in
688 Mediterranean sediments by a consortium of methanogenic archaea and bacteria.
689 The Medinaut Shipboard Scientific Party. Applied and Environmental Microbiology
690 66, 1126-1132.

691 Paull, C.K., Ussler III, W, 2006. Re-evaluating the significance of seafloor
692 accumulations of methane-derived carbonates: seepage or erosion indicators?
693 Proceedings of the 6th International Conference on Gas Hydrates, Vancouver,
694 Canada.

695 Paull. C.K., Ussler III, W., Peltzer, E.T., Brewer, P.G., Keaten, R., Mitts, P.J., Nealon,
696 J.W., Greinert, J., Herguera, J.C. & Perez, M.E. 2007. Authigenic carbon entombed
697 in methane-soaked sediments from the northeastern transform margin of the
698 Guayamas Basin, Gulf of California. Deep-Sea Research II, 54, 1240-1267.

699 Peckmann J., Reimer A., Luth U., Luth C., Hansen B.T., Heinicke C., Hoefs, J.
700 Reitner, J. 2001. Methane-derived carbonates and authigenic pyrite from the
701 northwestern Black Sea. Marine Geology 177, 129-150.

702 Peckmann, J., Thiel, V. 2004. Carbon cycling at ancient methane seeps.
703 Chemical Geology 205, 443-467.

704 Pierre, C., Fouquet, Y. 2007. Authigenic carbonates from methane seeps of the Congo
705 deep-sea fan. Geo-Marine Letters 27, 249-257.

706 Rathburn, A.E., Levin, L.A., Held, Z., Lohmann, K.C. 2000. Benthic foraminifera
707 associated with cold methane seeps on the northern California margin: ecology and
708 stable isotope composition. Marine Micropaleontology 28, 247-266.
709 Reitner, J., Peckmann, J., Reimer, A., Schumann, G., Theil, V. 2005. Methane-
710 derived carbonate build-ups and associated microbial communities at cold seeps on
711 the lower Crimean shelf (Black Sea). Facies 51, 66-79.
712 Ritger, S., Carson, B., Suess, E. 1987. Methane-derived authigenic carbonates formed
713 by subduction-induced pore-water expulsion along the Oregon/Washington margin.
714 Geological Society of America Bulletin 98, 147-156.
715 Rütters, H., Sass, H., Cypionka, H., Rullkötter, J. 2001. Monoalkylether
716 phospholipids in the sulfate-reducing bacteria *Desulfosarcina variabilis* and
717 *Desulforhabdus amnigenus*. Archives of Microbiology 176, 435-442.
718 Sackett, W.M. 1978. Carbon and hydrogen isotope effects during the thermocatalytic
719 production of hydrocarbons in laboratory simulation experiments. Geochemica et
720 Cosmochemica Acta 42, 571-580.
721 Schmidt, M., Botz, R., Winn, K., Stoffers, P., Thiessen, O., Herzig, P. 2002. Seeping
722 hydrocarbons and related carbonate mineralization in sediments south of Lihir Island
723 (New Ireland fore arc basin, Papua New Guinea). Chemical Geology 2002, 249-264.
724 Sibuet, M., Olu, K. 1998. Biogeography, biodiversity and fluid dependence of deep-
725 sea cold-seep communities at active and passive margins. Deep-Sea Research II 45,
726 517-567.
727 Stakes, D.S., Orange, D., paduan, J.B., Salamy, K.A., Maher, N. 1999. Cold seeps and
728 authigenic carbonate formation in Monterey Bay, California. Marine Geology 159,
729 93-109.

730 Svensen, H., Planke, S., Sørenssen, A.-M., Jamtveit, B., Myklebust, R., Eidem, T.R.,
731 Rey, S.S. 2004. Release of methane from a volcanic basin as a mechanism for initial
732 Eocene global warming. Nature 429, 542-545.
733 Tsunogai, U., Yoshida, N., Gamo, T. 2002. Carbon isotopic evidence of methane
734 oxidation through sulfate reduction in sediment beneath cold seep vents on the
735 seafloor at Nankai Trough. Marine Geology 187, 145-160.
736 Ulrich, G., Bower, S. 2008. Active methanogenesis and acetate utilization in Powder
737 River Basin coals, United States. International Journal of Coal Geology 76, 25-33.
738 van Dover, C.L., Aharon, P., Bernhard, J.M., Caylor, E., Doerries, M., Flickinger, W.,
739 Gilhooly, W., Goffredi, S.K., Knick, K.E., Macko, S.A., Rapaport, S., Raufls, E.C.,
740 Ruppel, C., Salerno, J.L., Seitz, R.D., Sen Gupta, B.K., Shank, T., Turnipseed, M. &
741 Vrijenhoek, R. 2003. Blake Ridge methane seeps: characterization of a soft-sediment,
742 chemosyntetically based ecosystem. Deep-Sea Research I 50, 281-230.
743 Valentine, D.L., Reeburgh, W.S. 2000. New perspectives on anaerobic methane
744 oxidation. Environmental Microbiology 2, 477-484.
745 von Rad, U., Rösch, H., Berner, U., Geyh, M., Marchig, V., Schulz, H. 1996.
746 Authigenic carbonates derived from oxidized methane vented from the Makran
747 accretionary prism off Pakistan. Marine Geology 136, 55-77.
748 Walter, L.M. 1986. Relative efficiency of carbonate dissolution and precipitation
749 during diagenesis: a progress report on the role of solution chemistry, in: Gauties,
750 D.L. (Ed.), Roles of organic matter in mineral diagenesis, SEPM (Society for
751 Sedimentary Geology) Special Publication 38, 1-12.
752 Whiticar, M.J. 1999. Carbon and hodrogen isotope systematics of bacterial formation
753 and oxidation of methane. Chemical Geology 161, 291-314.

754 Whomersley, P., Wilson, C., Clements, A., Brown, C., Long, D., Leslie, A.,
755 Limpenny, D. 2010. Understanding the marine environment - seabed habitat
756 investigation of submarine structures in the mid Irish Sea and Solan Bank Area of
757 Search (AoS). JNCC Report No. 430.

758 Yuan, F., Bennell, J., Davis, A. 1992. Acoustic and physical characteristics of gassy
759 sediments in the western Irish Sea. Continental Shelf Research 12, 1121-1134.

760

761

762 **Tables and Figures**

763 Table 1. Summary data of collected cemented carbonates from the Codling Fault Zone.

764 Table. 2. Stable isotope composition of the sample PMO 217.327-109 from site G109.

765

766 Fig. 1. The Codling Fault Zone mound features (white arrows), sampling stations (white crosses),
767 underwater video tracklines (dark grey lines), and captured image stills of exposed carbonates or black
768 reduced sediment (white stars). A. Location of the area of study. B. A 3D Fledermaus image showing
769 the topography of some of the mounds features.

770

771 Fig. 2. Underwater towed video (A to F) and grab sampling (G to I) of Codling Fault mound targets. A.
772 Semi-exposed nodules and pavement (P1). B. Semi-exposed hardgrounds (P2). C. Pavement stacking
773 (P3). D. Reduced surface sediment (P4). E. Large exposed hardgounds (P5). F. Exposed colonised and
774 non-colonised hardgrounds (P6). G. G103. H. G107. I. G109, a hardground colonised by a *Nemertesia*
775 hydroid. Unlabelled scale bars = 25cm. The locations for underwater still images and sampling stations
776 are given in Fig. 1 and Table 1.

777

778 Fig. 3. Single beam echosounder profile showing topography of mound features and active gas seepage
779 to the water column from close to its apex. The location of the mound is shown in Fig. 1.

Fig. 4. A, B. Representative SEM-EDS analyses of the composition of sampled hard grounds. C. SEM micrograph showing carbonate-cemented quartz grain. D. Aragonite crystals and framboidal pyrite. E. Detail of framboidal pyrite.

Fig. 5. Aragonite cemented allochemic sandstone with bioclasts (G109). All microphotographs from PMO 217.327. A. Low magnification view of petrographic thin section; transmitted light. Note the large contribution of quartz grains in the rock volume. Empty cavities visible in the lover part of the picture are a product of sample preparation. B Detail showing a possible glaucony granule (black arrow) and an echinoderm skeletal fragment (grey arrow). C. Detail showing a bivalve fragment, possibly an oyster (black arrow), and a red algal fragment (grey arrow). D. Detail showing a balanid barnacle fragment (black arrow). E. Detail showing a gastropod (black arrow) and a possible foraminiferan (grey arrow). F. Same area as in E in polarized light.

Fig. 6. X-ray powder diffractogram of sample PMO 217.327. The blue rhombi represent quartz, red squares represent aragonite and red triangles represent Mg-calcite.

Fig. 7. Carbon and oxygen stable isotope data from sample PMO 217.327. Regression line in red.

Fig. 8. Total ion chromatograms of a representative phospholipid fatty acid sample (A) and an alcohol fraction (B) from extracted aragonite-cemented quartz (G109 and G. Major compounds are labeled. Fatty acid nomenclature is according to *X:Y*ω*Z*, where *X* refers to the number of carbon atoms present, *Y* refers to the number of double bonds on the carbon chain and *Z* refers to the position of the first double bond from the methyl end. Sterol nomenclature is according to $C_X\Delta^Y$ where *Y* refers to the position of double bond(s) on the sterol skeleton.

Fig. 9. Measured $\delta^{13}C$ values for selected biomarkers extracted from samples G103, G107 and G109. See Fig. 1. for station location. IS = internal standard (5-α-cholestane).

Figure

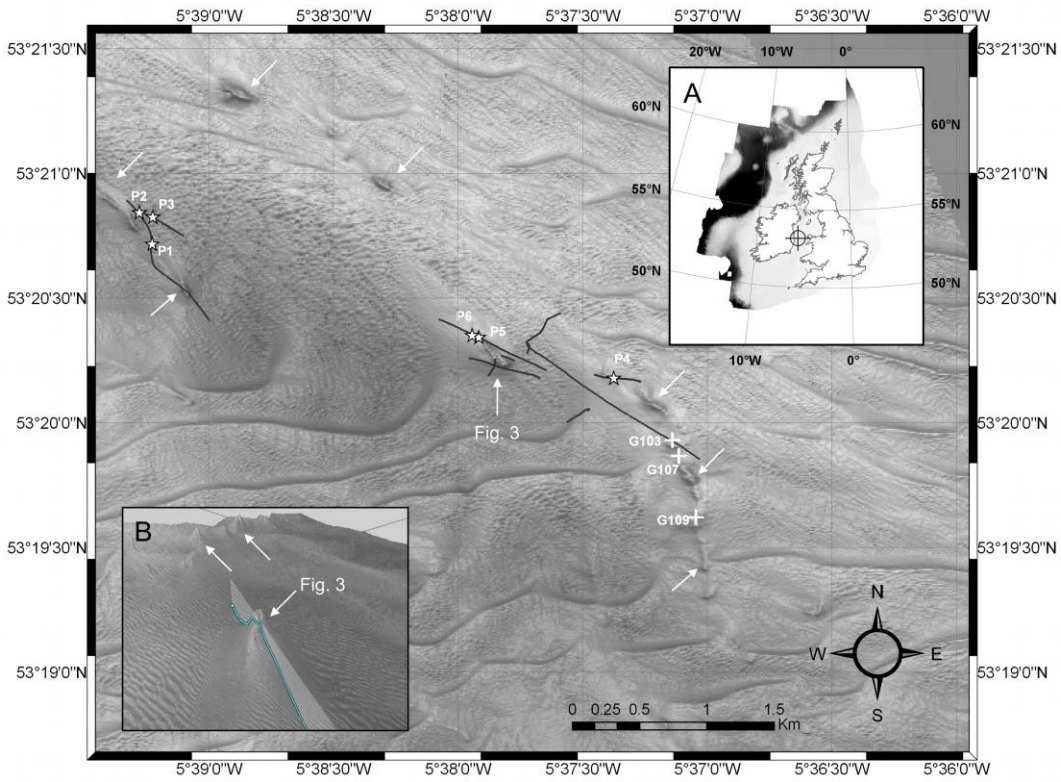

Fig. 1. The Codling Fault Zone mound features (white arrows), sampling stations (white crosses), underwater video tracklines (dark grey lines), and captured image stills of exposed carbonates or black reduced sediment (white stars). A. Location of the area of study. B. A 3D Fledermaus image showing the topography of some of the mounds features.

Figure

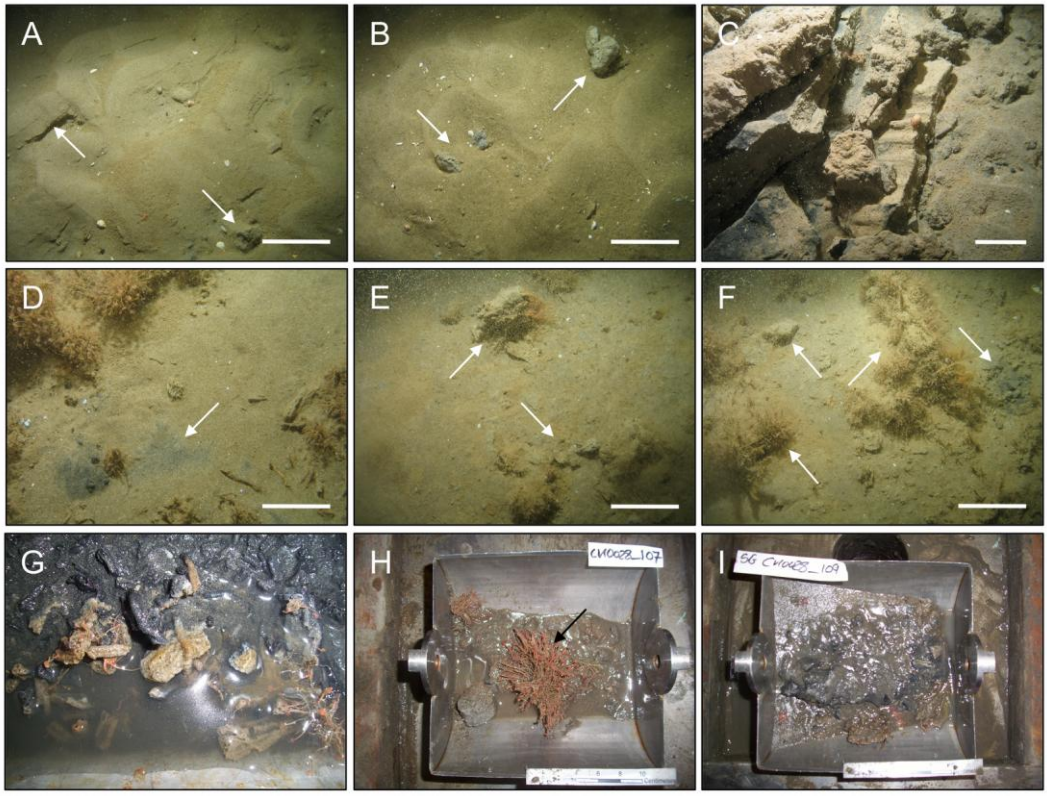

Fig. 2. Underwater towed video (A to F) and grab sampling (G to I) of Codling Fault mound targets. A. Semi-exposed nodules and pavement (P1). B. Semi-exposed hardgrounds (P2). C. Pavement stacking (P3). D. Reduced surface sediment (P4). E. Large exposed hardgounds (P5). F. Exposed colonised and non-colonised hardgrounds (P6). G. G103. H. G107. I. G109, a hardground colonised by a *Nemertesia* hydroid. Unlabelled scale bars = 25cm. The locations for underwater still images and sampling stations are given in Fig. 1 and Table 1.

Figure

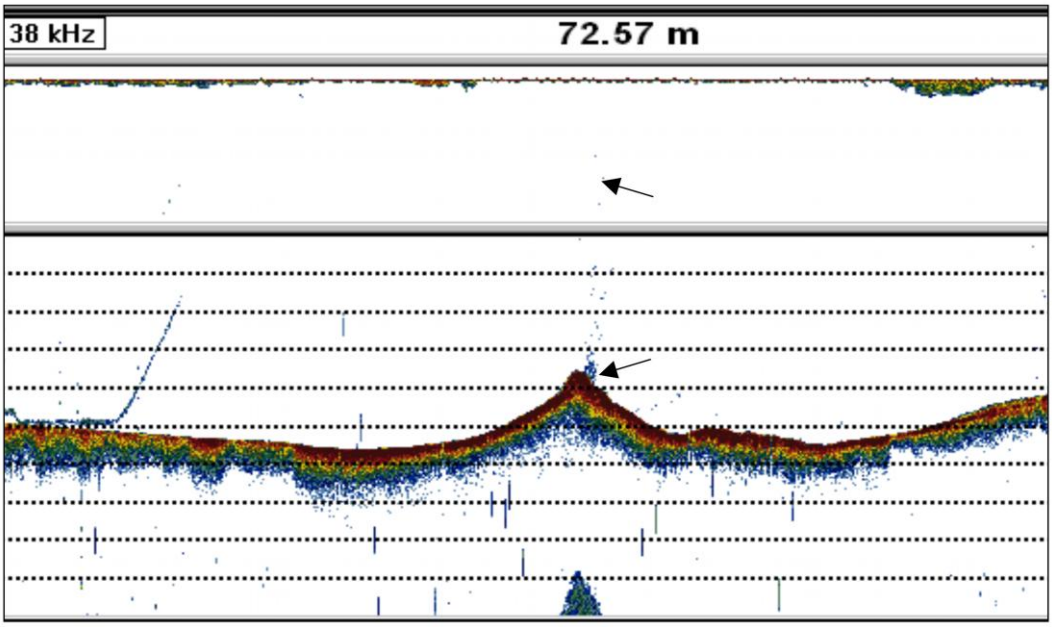

Fig. 3. Single beam echosounder profile showing topography of mound features and active gas seepage to the water column from close to its apex. The location of the mound is shown in Fig. 1.

Figure

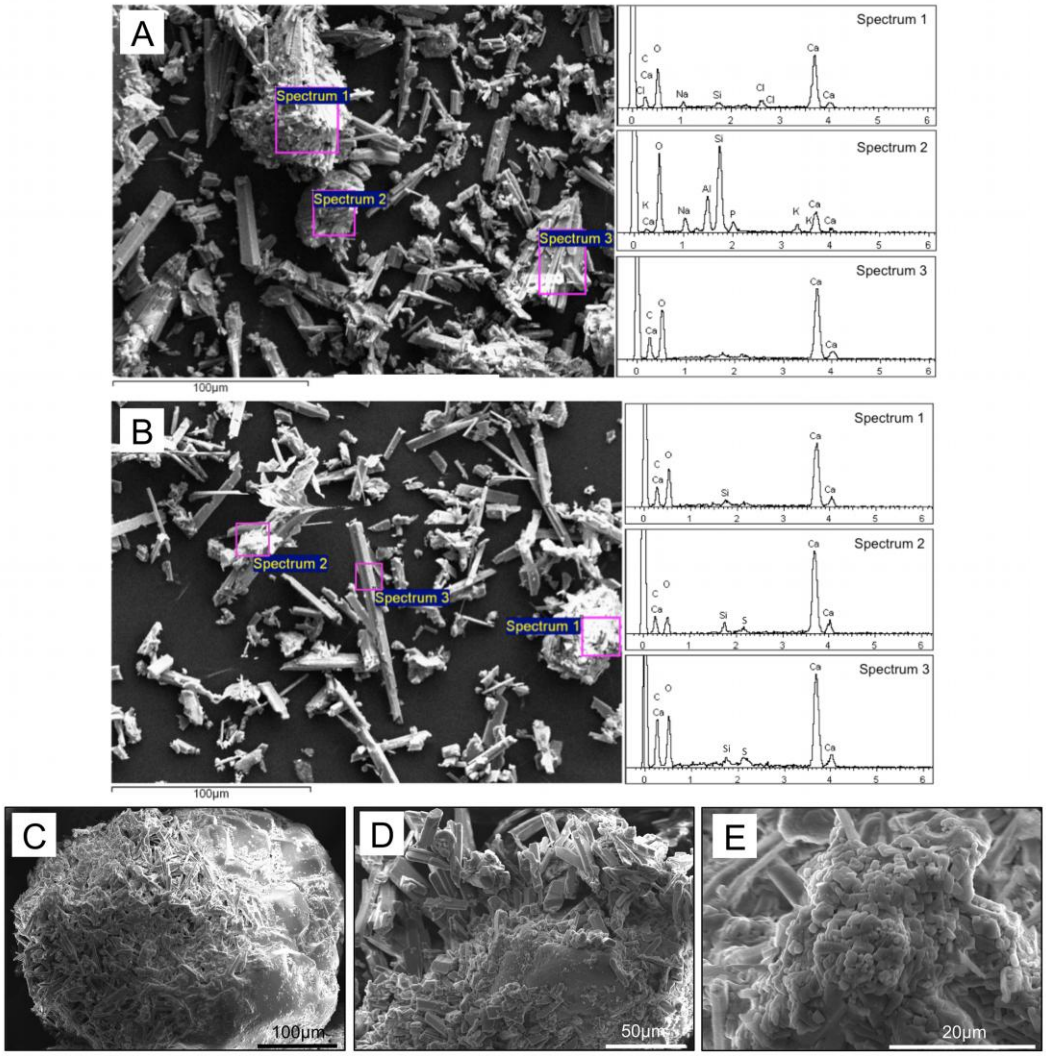

Fig. 4. A, B. Representative SEM-EDS analyses of the composition of sampled hard grounds. C. SEM micrograph showing carbonate-cemented quartz grain. D. Aragonite crystals and framboidal pyrite. E. Detail of framboidal pyrite.

Figure

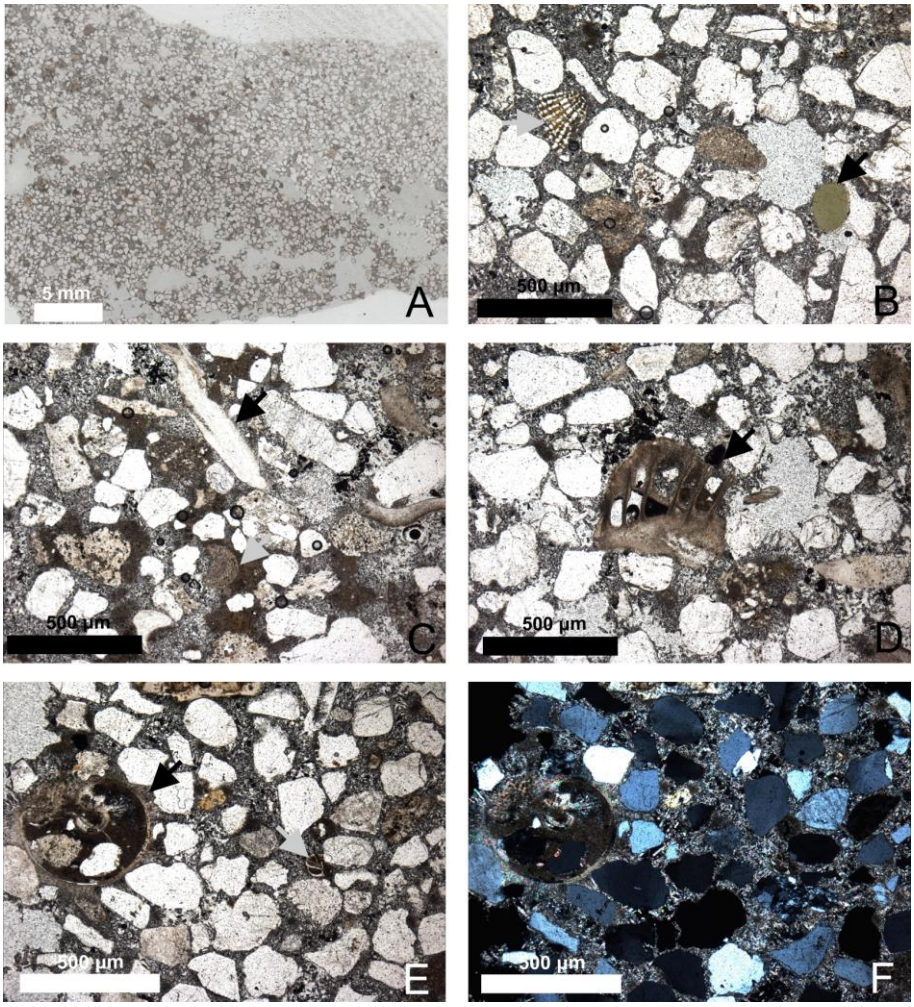

Fig. 5. Aragonite cemented allochemic sandstone with bioclasts (G109). All microphotographs from PMO 217.327. A. Low magnification view of petrographic thin section; transmitted light. Note the large contribution of quartz grains in the rock volume. Empty cavities visible in the lover part of the picture are a product of sample preparation. B Detail showing a possible glaucony granule (black arrow) and an echinoderm skeletal fragment (grey arrow). C. Detail showing a bivalve fragment, possibly an oyster (black arrow), and a red algal fragment (grey arrow). D. Detail showing a balanid barnacle fragment (black arrow). E. Detail showing a gastropod (black arrow) and a possible foraminiferan (grey arrow). F. Same area as in E in polarized light.

Figure

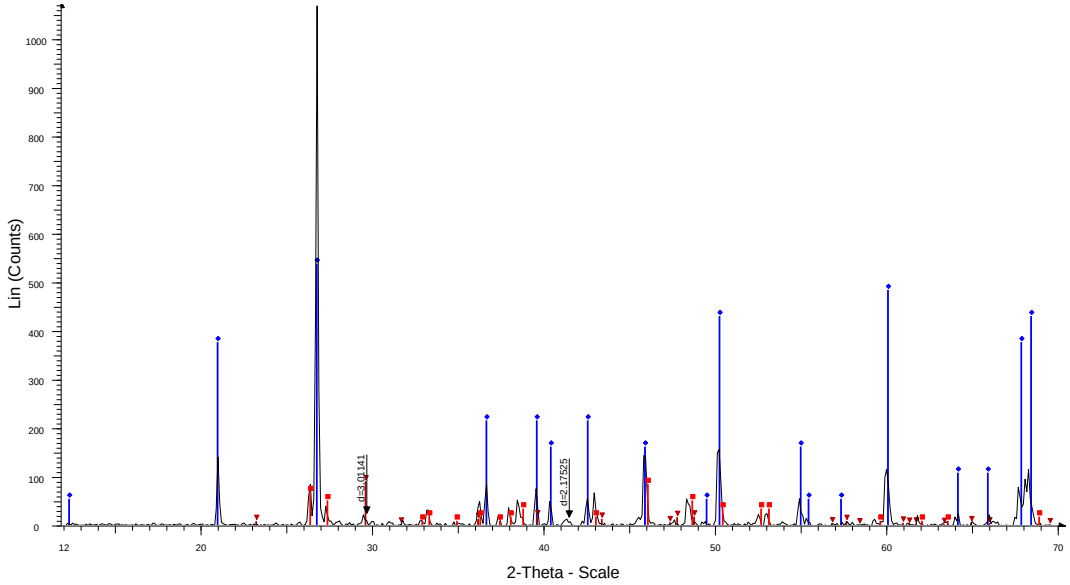

Fig. 6. X-ray powder diffractogram of sample PMO 217.327. The blue rhombi represent quartz, red squares represent aragonite and red triangles represent Mg-calcite.

Figure

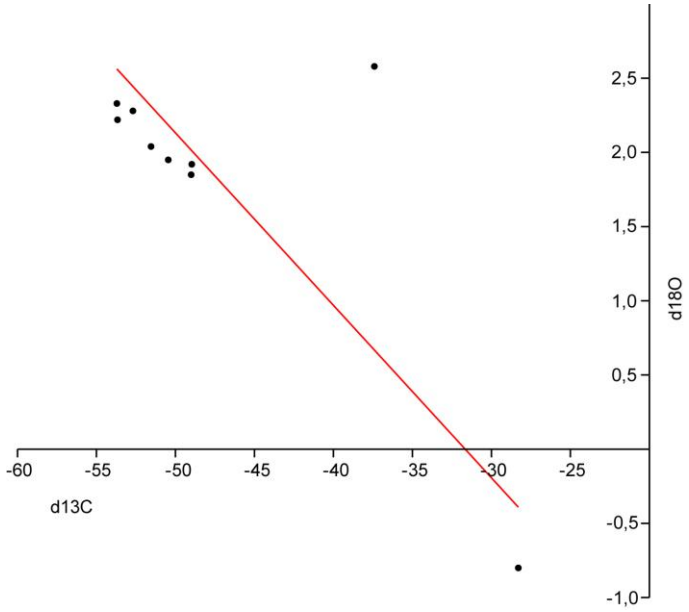

Fig. 7. Carbon and oxygen stable isotope data from sample PMO 217.327. Regression line in red.

Figure

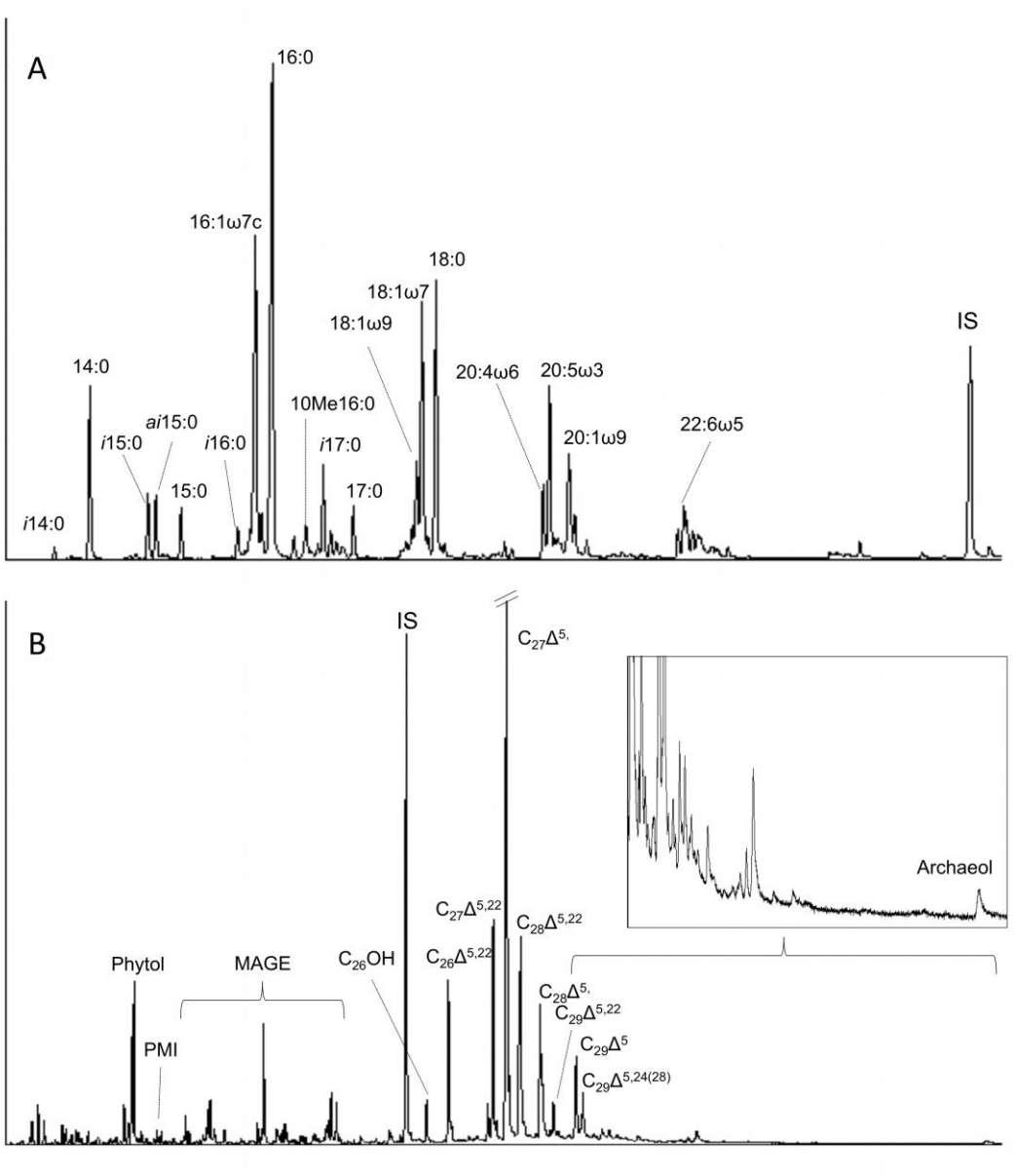

Fig. 8. Total ion chromatograms of a representative phospholipid fatty acid sample (A) and an alcohol fraction (B) from extracted aragonite-cemented quartz (G109 and G. Major compounds are labeled. Fatty acid nomenclature is according to *X:Y*ω*Z*, where *X* refers to the number of carbon atoms present, *Y* refers to the number of double bonds on the carbon chain and *Z* refers to the position of the first double bond from the methyl end. Sterol nomenclature is according to $C_X\Delta^Y$ where *Y* refers to the position of double bond(s) on the sterol skeleton.

Figure

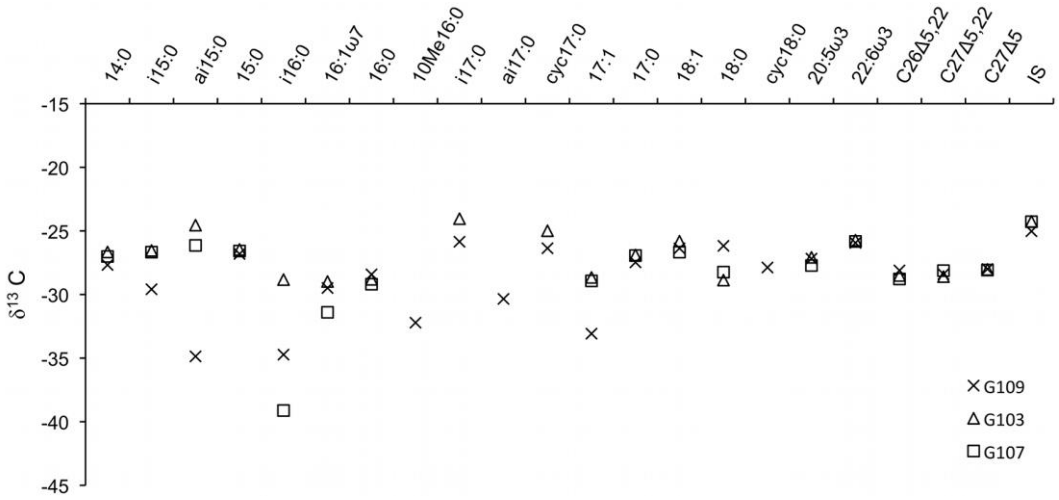

Fig. 9. Measured $\delta^{13}C$ values for selected biomarkers extracted from samples G103, G107 and G109. See Fig. 1. for station location. IS = internal standard (5-α-cholestane).

Table

Click here to download Table: Table 1.docx

Table 1. Summary data of collected cemented carbonates from the Codling Fault Zone.

Station		G103	G107	G109
Latitude		53°19'55"N	53°19'51"N	53°19'35"N
Longitude		5°37'9" W	5°37'7"W	5°37'4"W
Water Depth (m)		58	61	67
Sediment		Black reducing coarse sand, hydroids,	Dark greyish brown sand, hydroids	Dark greyish brown sand and black reducing
Hardgrounds (approx. %)		Cemented worm tubes (70%)	20%	50%
E_h (mV)		-177	-	-
Bulk $\delta^{13}C$ (‰)		-	-36.97	-53.71 to -28.30
Bulk $\delta^{18}O$ (‰)		-	3.54	-0.80 to 2.58
Major Elements (%)		Ca (68), Si (15), Al (5), Na (4)	Si (59), Ca (37), Cl (4)	Ca (96), Si (4)
Fatty acids (μg g^{-1})		1.11	1.58	3.4
(%)	SATFA[1]	32.7	35.7	39.1
	MUFA[2]	37.6	25	33.2
	PUFA[3]	13.5	27.7	16.7
	brFA[4]	16.2	11.7	11
	$iC_{15:0}$	2.7	1.1	1.8
	$aiC_{15:0}$	2	0.6	1.8
	$C_{16:1\omega5}$	1.7	0.6	1.3
	$10MeC_{16:0}$	3.2	1.9	1.1
	$iC_{17:0}$	1.8	1.2	2.5
	$aiC_{17:0}$	0.6	0.6	0.7
	$C_{17:1\omega6}$	0.6	n.d.	0.3
	$cycC_{17:0}$	0.8	0.4	0.4
	$cycC_{18:0}$	0.6	n.d.	0.4
Sterols (μg g^{-1})		1.32	4.46	1.72
(%)	C_{26}	9.8	9.9	6.8
	C_{27}	69.1	70.9	59.8
	C_{28}	15	14.3	22.4
	C_{29}	6.2	4.8	11
n-alkanols (ng g^{-1})[5]		19	24	47
MAGE (ng g^{-1})[6]		49	36	161
Phytol (ng g^{-1})		n.d.	n.d.	22
Crocetane (ng g^{-1})[7]		<1	n.d.	1
PMI (ng g^{-1})[8]		9	n.d.	10
Archaeol (ng g^{-1})		1	n.d.	7

1. Saturated fatty acids
2. Monounsaturated fatty acids
3. Polyunsaturated fatty acids
4. Branched (including cyclic) fatty acids
5. C_{14} to C_{26} *n*-alkanols
6. Monoalkyl glyceryl ethers ranging from C_{14} to C_{20}
7. Co-eluting – concentrations estimated based on abundance of key m/z fragments
8. Pentamethyleicosane

Table

Click here to download Table: Table 2.docx

Table. 2. Stable isotope composition of the sample PMO 217.327-109 from site G109.

Number of sample	$\delta^{13}C$	$\delta^{18}O$
PMO 217.327-1	51,55	2,04
PMO 217.327-2	50,46	1,95
PMO 217.327-3	48,97	1,92
PMO 217.327-4	53,67	2,22
PMO 217.327-5	28,30	-0,80
PMO 217.327-6	52,70	2,28
PMO 217.327-7	37,41	2,58
PMO 217.327-8	53,71	2,33
PMO 217.327-9	49,01	1,85